Electronic Supplementary Material (ESI) for Dalton Transactions.

Supporting information for

Reversible Al^{3+} ion insertion in WO_3 for aqueous aluminum-ion battery

Homen Lahan[a], Shyamal K. Das[#a]

[a] Department of Physics, Tezpur University, Assam 784028, India

Experimental details:

Synthesis of WO_3: WO_3 was synthesized by adopting a hydrothermal method as reported in Ref. [S1]. In a typical synthesis, 0.825 g of sodium tungstate ($Na_2WO_4.2H_2O$) and 0.290 g of NaCl is mixed properly in 19 ml of distilled water followed by addition of 3 M HCl solution in order to attain a pH value of 2. The solution is then transferred into a teflon lined stainless steel autoclave and kept at 180 ^{O}C for 24 h and then cooled to room temperature. The resultant product was recovered by centrifugation and washed with deionized water and ethanol several times and dried at 110 ^{o}C for 12 h.

Characterization: The crystallographic phase identification was performed by using powder X-ray diffraction (BRUKER AXS D8 FOCUS; Cu-K_α radiation, λ = 1.5406 Å). Raman spectra are obtained from RENISHAW BASIS SERIES having 514 laser excitation. The morphology was observed by scanning electron microscopy (SEM, JEOL JSM 6390LV).

Electrochemical Analysis: Electrode slurries were made from active material (WO_3), polyvinylidene fluoride and N-methyl-2-pyrrolidone. The weight ratio of WO_3 and polyvinylidene fluoride is 80:20. The slurry was cast on graphite film and dried at 120 ^{o}C for 12

[#] *Corresponding author; email: skdas@tezu.ernet.in; Tel: +91-3712275586; Fax: +91-3712267005*

h. The cyclic voltammetry and galvanostatic cycling experiments were performed in a conventional three-electrode electrochemical cell using Biologic SP300 electrochemical work station. Pt electrode and aqueous Ag/AgCl electrode were used as the counter and reference electrodes respectively. The utilized electrolytes were 1 M $AlCl_3$, 1 M $Al(NO_3)_3$, 0.5 M $Al_2(SO_4)_3$, 1 M LiCl, 1 M NaCl and 1 M $MgCl_2$ aqueous solutions. Extreme care must be taken while mixing $AlCl_3$ in H_2O because the reaction is exothermic and reacts very violently particularly at higher molar concentrations. The $Al_2(SO_4)_3$ concentration was maintained at 0.5 M because it could not be dissolved beyond 0.5 M in water. The discharge/charge and CV experiments were performed in the voltage range of -0.9 V to 0.5 V. All the electrochemical experiments were conducted at room temperature (25 ^{o}C). For ex-situ XRD and SEM experiments, the electrodes were harvested after required discharge/charge cycles and washed with deionized water and dried at 110 ^{o}C for 24 h. Ex-situ UV-visible spectra were recorded for PVDF, pristine WO_3, WO_3 after 1st discharge in 1 M $AlCl_3$ aqueous electrolyte (or Al^{3+} ion intercalated WO_3), WO_3 after 1st discharge in 1 M HCl aqueous electrolyte (or H^+ intercalated WO_3). The materials were dried at 110 ^{o}C for 24 h prior to measurement.

Band-gap energy estimation:

Optical band-gap energy values were estimated from the UV-Vis spectra using the well-known and widely used Tauc equation [S2-S5]. According to Tauc equation, the photon energy ($h\upsilon$) is related to optical band gap energy ($\mathrm{E_g}$) of a semiconductor by the following relationship:

$$\alpha h\upsilon = \mathrm{A}(h\upsilon - \mathrm{E_g})^{\mathrm{n}} \ldots\ldots\ldots\ldots\ldots\ldots\ldots(1)$$

where α and A are absorption coefficient and optical transition dependent constant, respectively. The exponent “n” indicates the nature of optical transition in the semiconductor. For allowed indirect and direct optical transitions, the values of n are respectively 2 and 0.5.

Optical band gap energy can be estimated by extrapolating the linear portion near the onset on the plot of $(\alpha h\upsilon)^{1/n}$ versus $h\upsilon$. Considering the nature of optical transition in WO_3 as indirect transition [S6], the band gaps for pristine WO_3, Al^{3+} ion intercalated WO_3, H^+ intercalated WO_3 were evaluated as shown in figure S16. PVDF does not show any absorption as shown in figure S16 and since the concentration of PVDF in the electrode is very less, the effect of PVDF in the estimation of band-gap is assumed to be negligible.

Reference:

S1: J. Wang, E. Khoo, P.S. Lee and J. Ma, *J. Phys. Chem. C*, 2008, **112**, 14306.

S2: D. G. Barton, M. Shtein, R. D. Wilson, S. L. Soled, Enrique Iglesia, J. Phys. Chem. B **103**, 630 (1999).

S3: Feng Zheng, Min Guo* and Mei Zhang, Cryst. Eng. Comm, 2013, 15, 277–284

S4: Y. Zhang, Z. R. Tang, X. Fu, Y. J. Xu, ACS Nano **4**, 7303 (2010)

S5: W. Fan, Q. Lai, Q. Zhang, Y. Wang, J. Phys. Chem. C **115**, 10694 (2011)

S6: P. P. González-Borrero, F. Sato, A. N. Medina, M. L. Baesso, A. C. Bento, G. Baldissera, C. Persson, G. A. Niklasson, C. G. Granqvist, A. F. da Silva, Applied Physics Letters, 96, 061909 (2010)

Supplementary figures

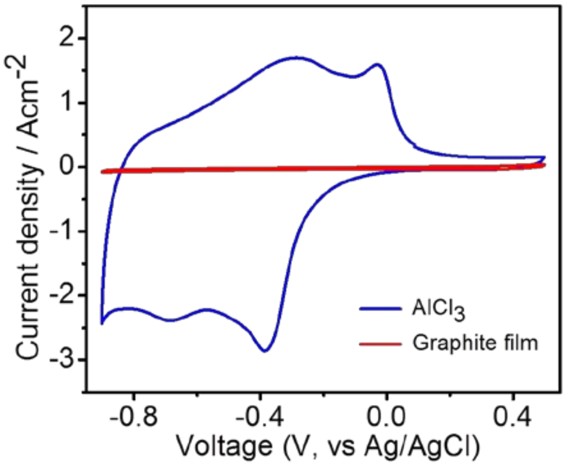

Figure S1. Comparison of CV curves of WO_3 and graphite foil in 1 M $AlCl_3$ aqueous electrolyte at a scan rate of 2.5 mVs^{-1}.

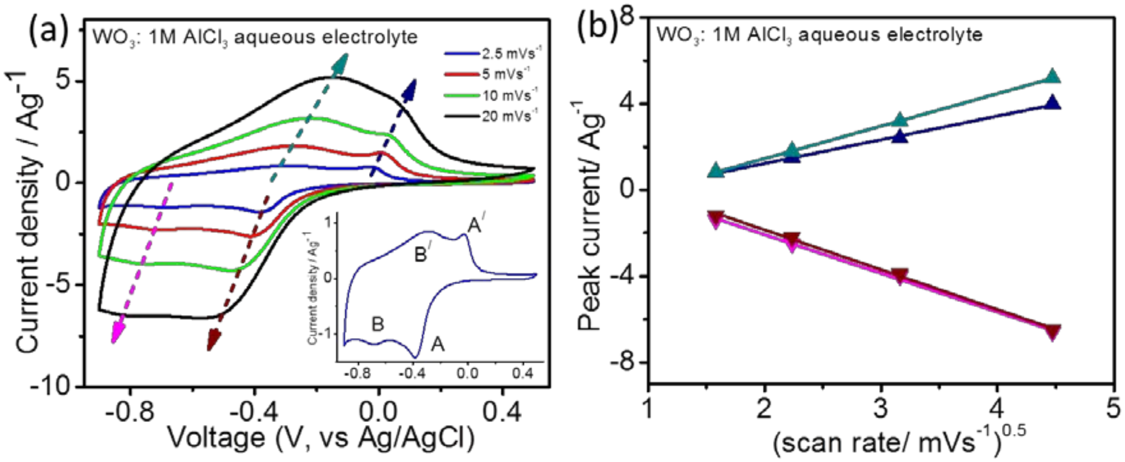

Figure S2: (a) CV curves of WO_3 in 1 M $AlCl_3$ aqueous electrolyte at different scan rates and (b) variation of redox peak current versus scan rate according to equation $I = k\gamma^{0.5}$ (see text for detail). The peaks marked by the arrows are considered here. Inset figure clearly shows the A, B, A$^{/}$, B$^{/}$ peaks for scan rate of 2.5 mVs^{-1}.

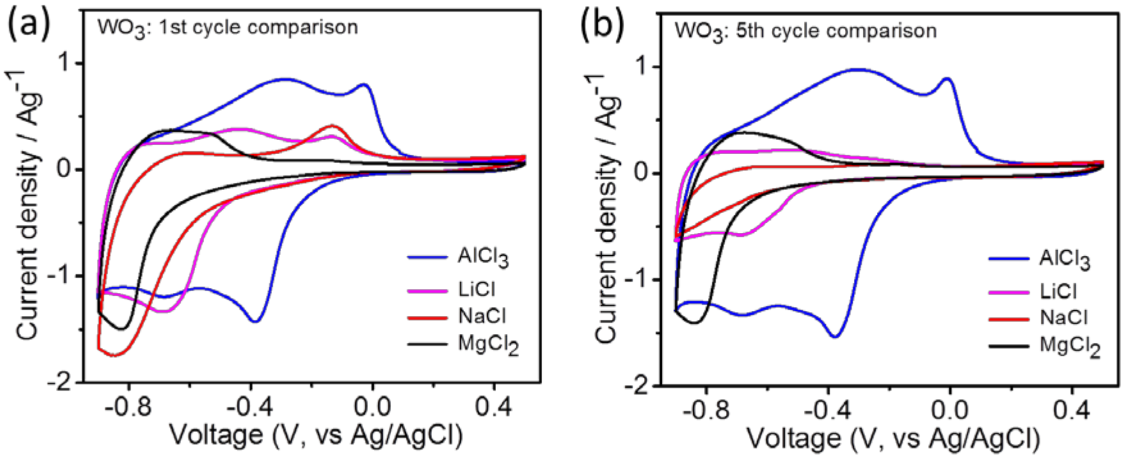

Figure S3: Comparison of CV curves of WO_3 obtained in 1 M $AlCl_3$, 1 M LiCl, 1 M NaCl and 1 M $MgCl_2$ aqueous electrolytes at a scan rate of 2.5 mVs^{-1}. (a) 1st cycle and (b) 5th cycle

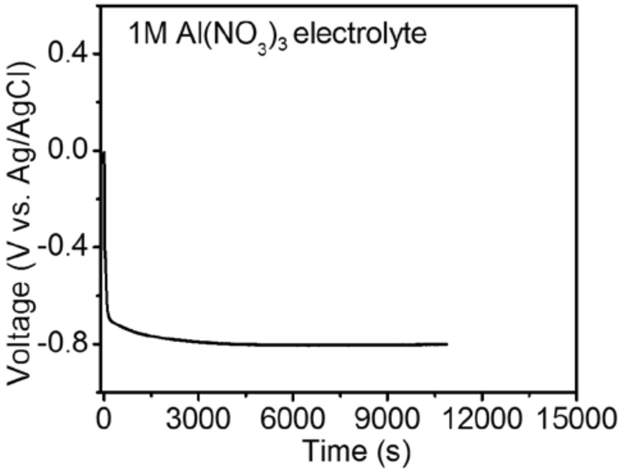

Figure S4: Galvanostatic discharge curve of WO_3 in 1 M $Al(NO_3)_3$ aqueous electrolyte at a current rate of 2.5 Ag^{-1} .

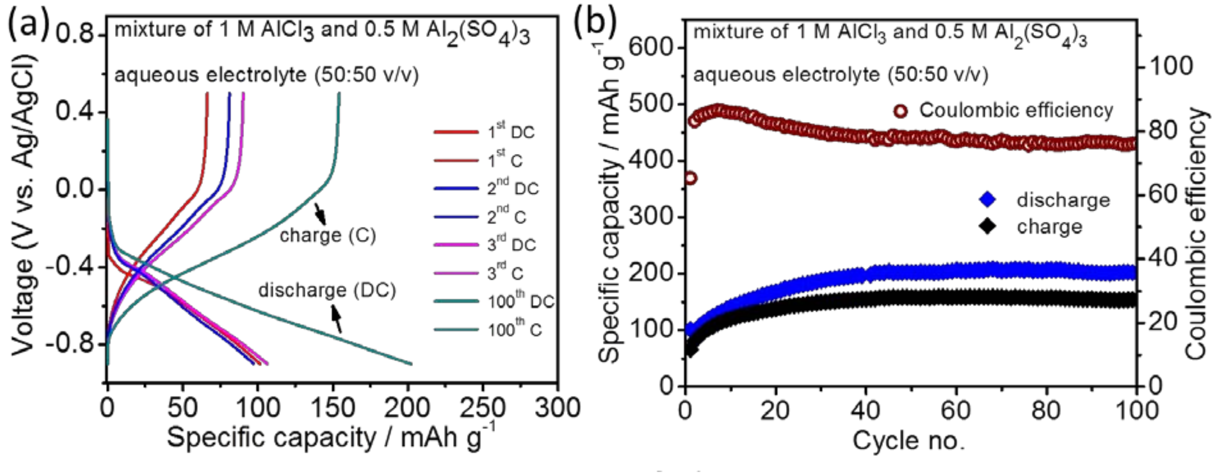

Figure S5: Galvanostatic discharge/charge curves of WO_3 in (a) 50:50 v/v mixture of 1 M $AlCl_3$ and 0.5 M $Al_2(SO_4)_3$ aqueous electrolytes, and (b) variation of specific capacities of WO_3 with cycle number. The current rate is 2.5 Ag^{-1}.

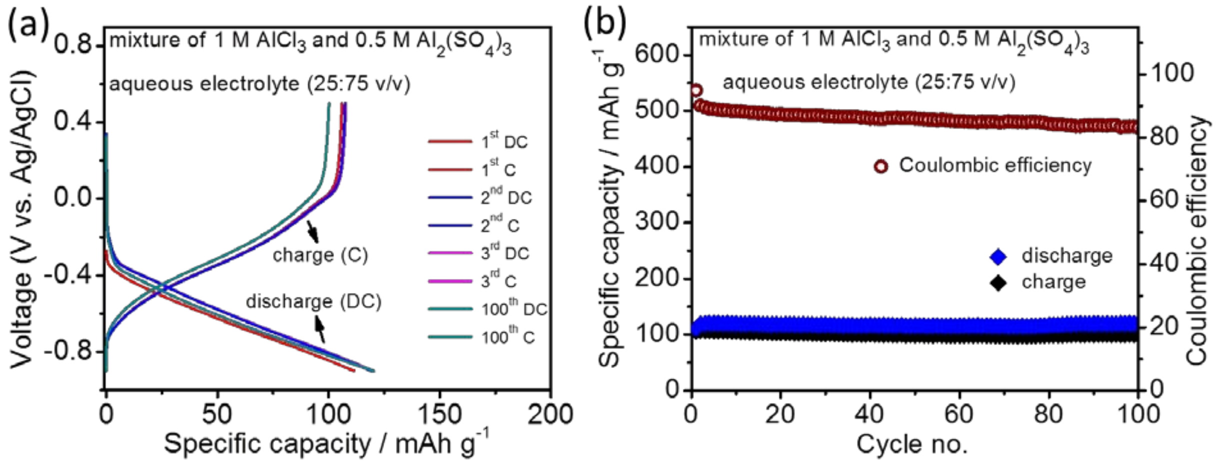

Figure S6: Galvanostatic discharge/charge curves of WO_3 in (a) 25:75 v/v mixture of 1 M $AlCl_3$ and 0.5 M $Al_2(SO_4)_3$ aqueous electrolytes, and (b) variation of specific capacities of WO_3 with cycle number. The current rate is 2.5 Ag^{-1}.

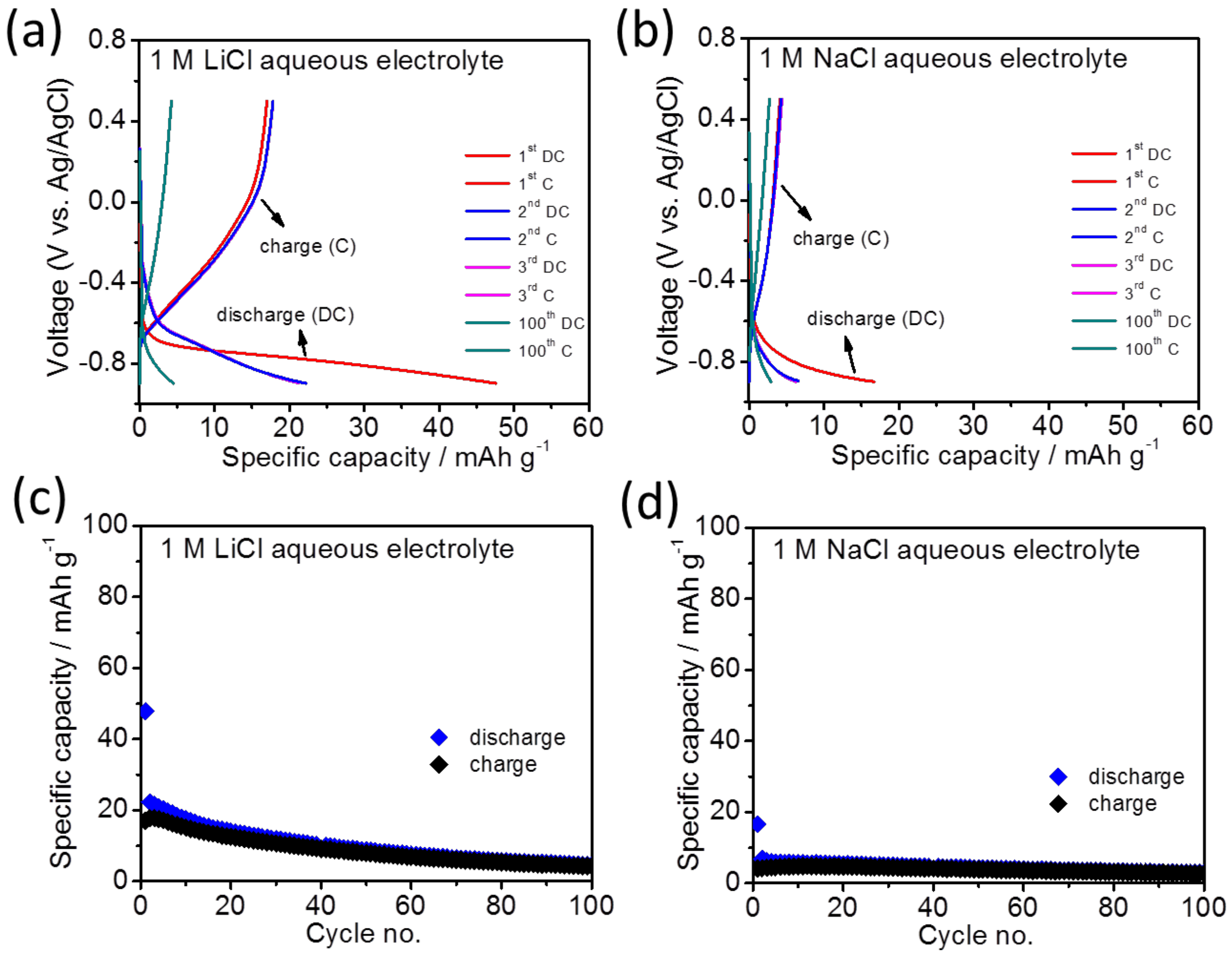

Figure S7: Galvanostatic discharge-charge profiles of WO_3 in (a) 1 M LiCl and (b) 1 M NaCl aqueous electrolytes. Variation of specific capacities of WO_3 with cycle number in (c) 1 M LiCl and (d) 1 M NaCl aqueous electrolytes. The current rate is 2.5 Ag^{-1}.

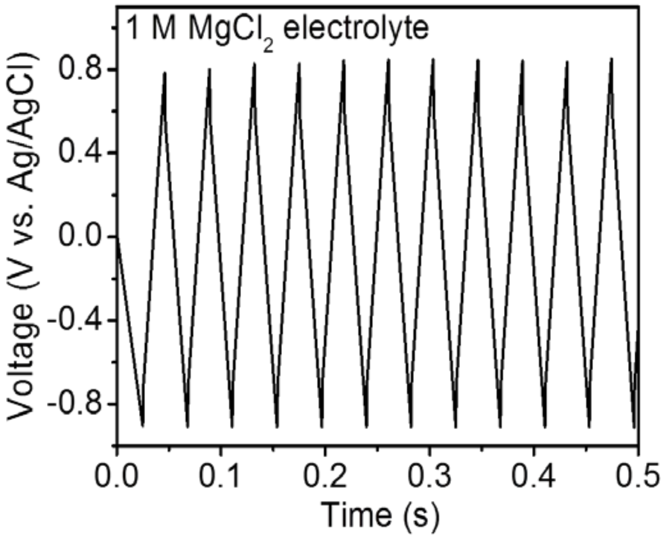

Figure S8: Galvanostatic discharge-charge profiles of WO_3 in 1 M $MgCl_2$ aqueous electrolyte at a current rate of 2.5 Ag $^{-1}$.

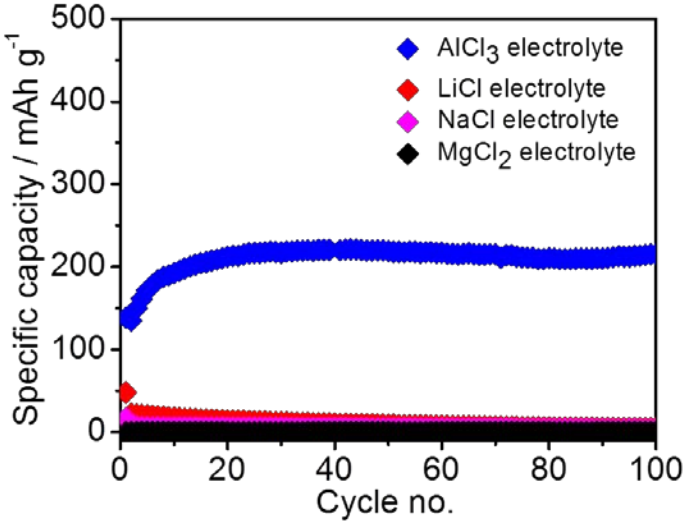

Figure S9: Comparison of discharge capacities in 1 M $AlCl_3$, 1 M LiCl, 1 M NaCl and 1 M $MgCl_2$ aqueous electrolytes at current rate of 2.5 Ag $^{-1}$.

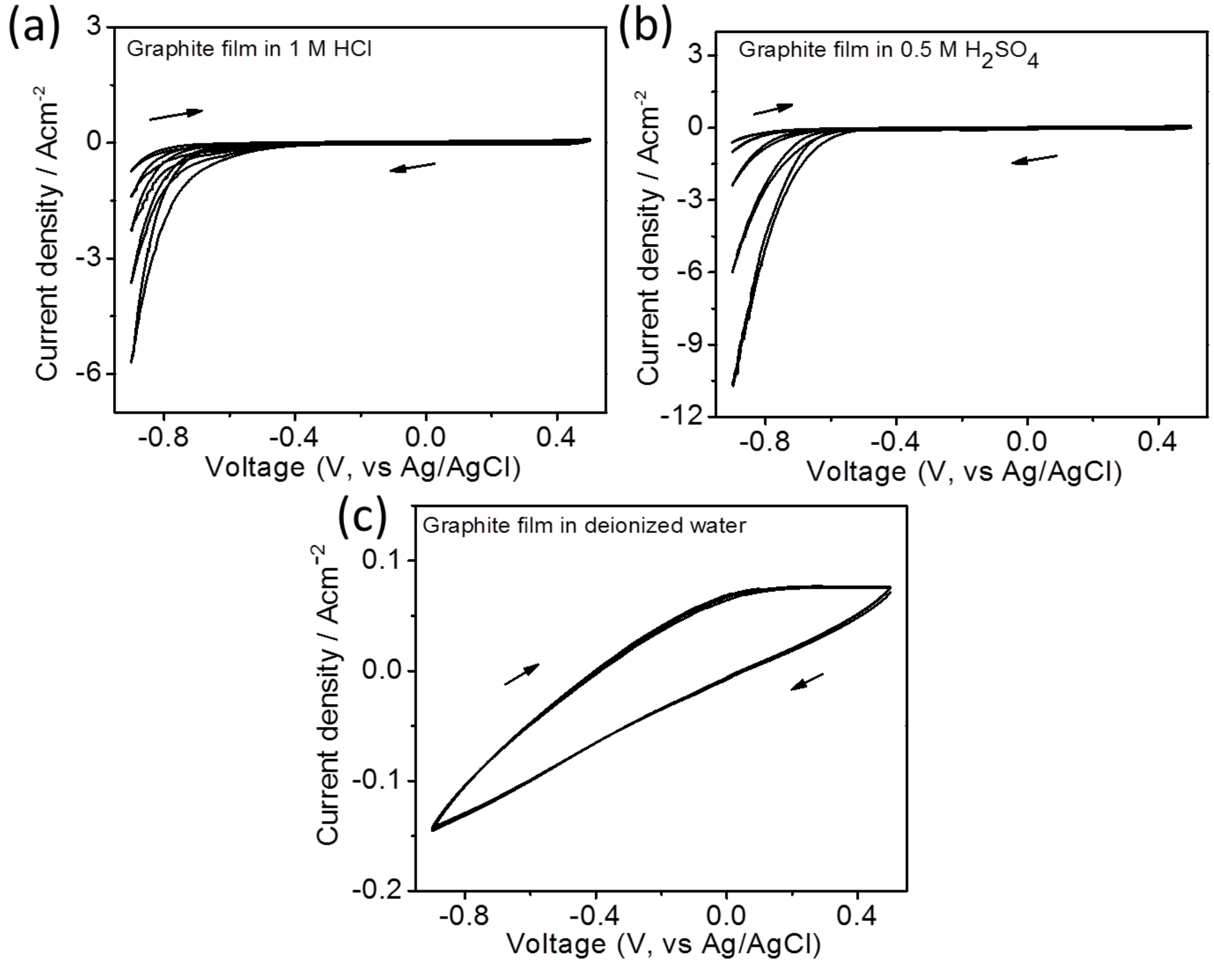

Figure S10: CV profiles of graphite film in (a) 1 M HCl, (b) 0.5 M H_2SO_4 and (c) deionized water at a scan rate of 2.5 mVs^{-1}.

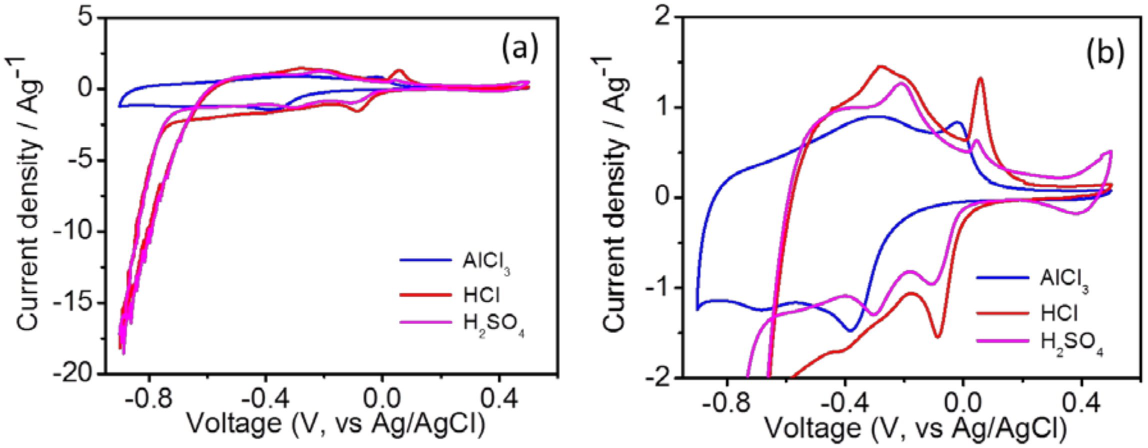

Figure S11: (a) Comparison of CV profiles of WO_3 in 1 M $AlCl_3$, 1 M HCl and 0.5 M H_2SO_4 electrolytes. (b) Enlarged view of figure a. The scan rate was 2.5 mVs^{-1} .

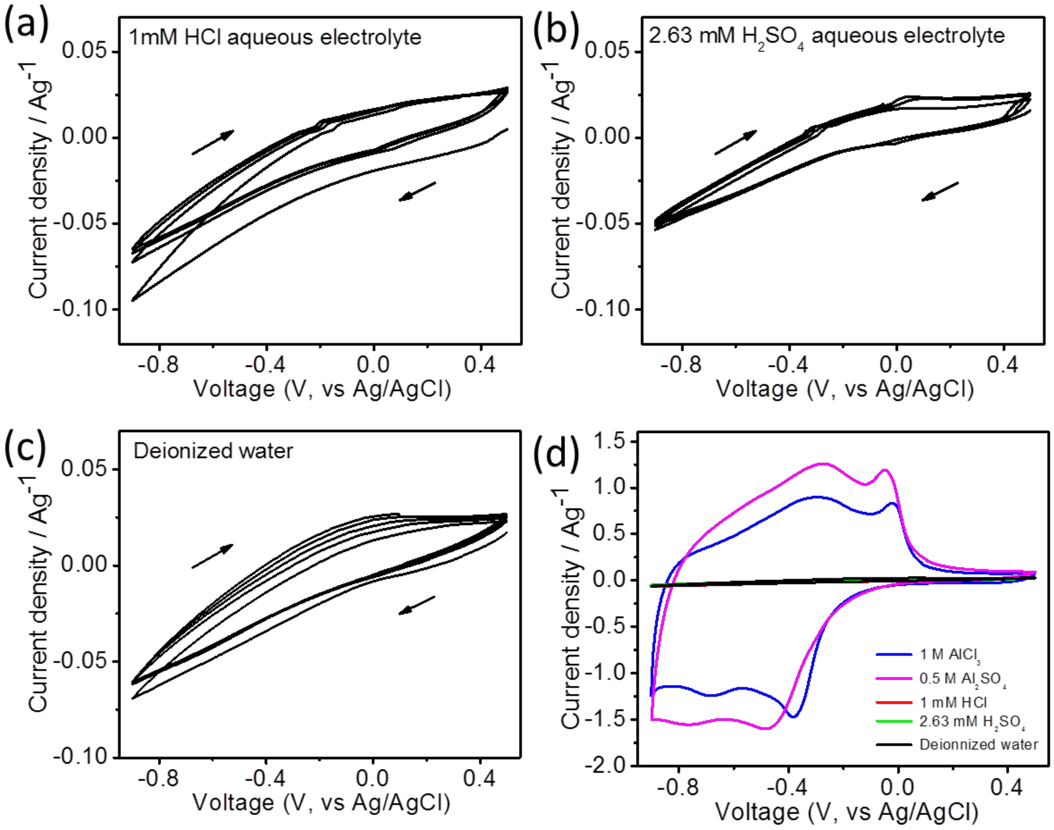

Figure S12: CV profiles of WO_3 in (a) 1 mM HCl, (b) 2.63 mM H_2SO_4 and (c) deionized water at a scan rate of 2.5 mVs^{-1}. (d) Comparison of these CV profiles with 1 M $AlCl_3$ and 0.5 M $Al_2(SO_4)_3$ aqueous electrolytes.

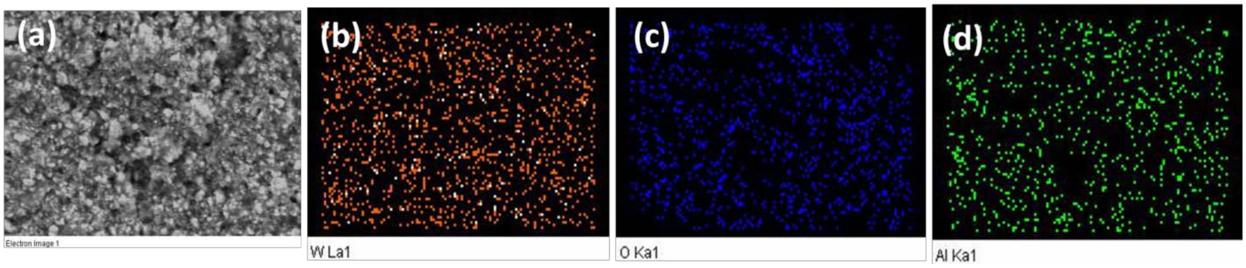

Figure S13: (a) SEM image of the scanned area for elemental mapping of 1st discharge state WO_3 electrode. Elemental mapping images of (b) W, (c) O and (d) Al of the 1st discharge state electrode.

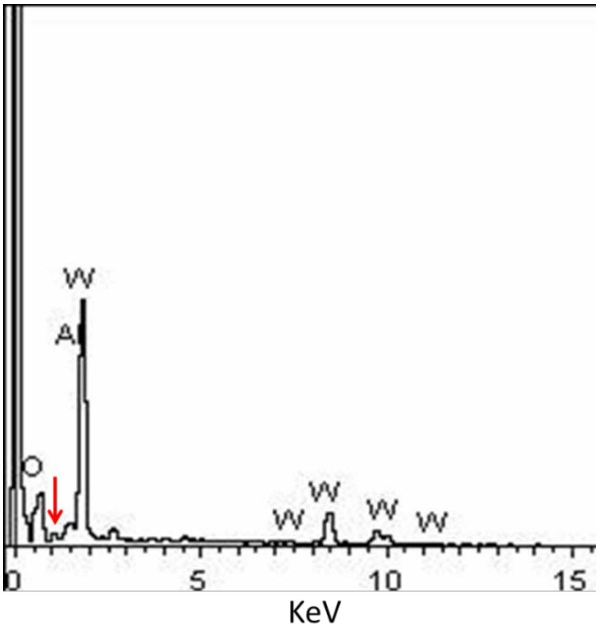

Figure S14: Energy dispersive X-ray (EDX) spectrum of 1st discharge state WO_3 electrode. The arrow shows the position for Al.

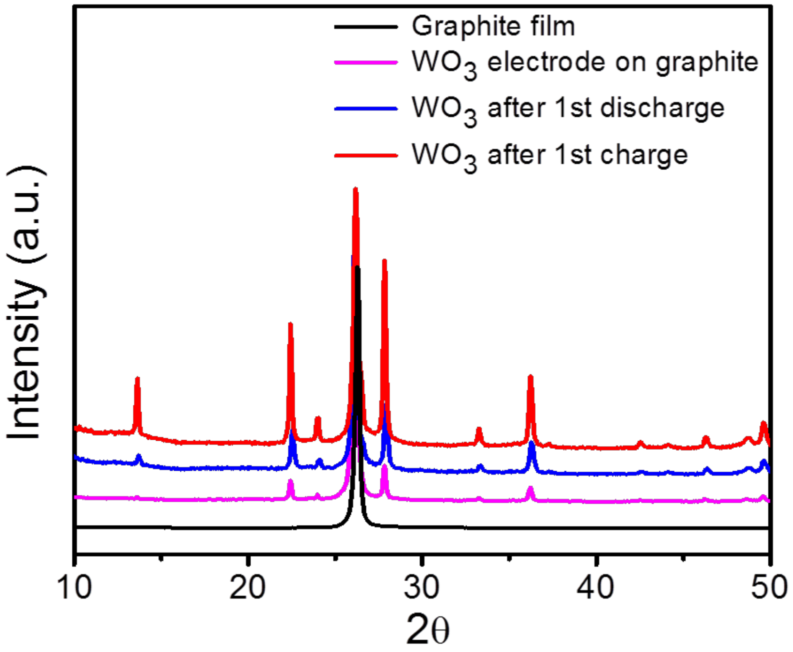

Figure S15: Ex-situ XRD patterns of graphite film, WO_3 electrode before discharge, after 1st discharge and after 1st charge.

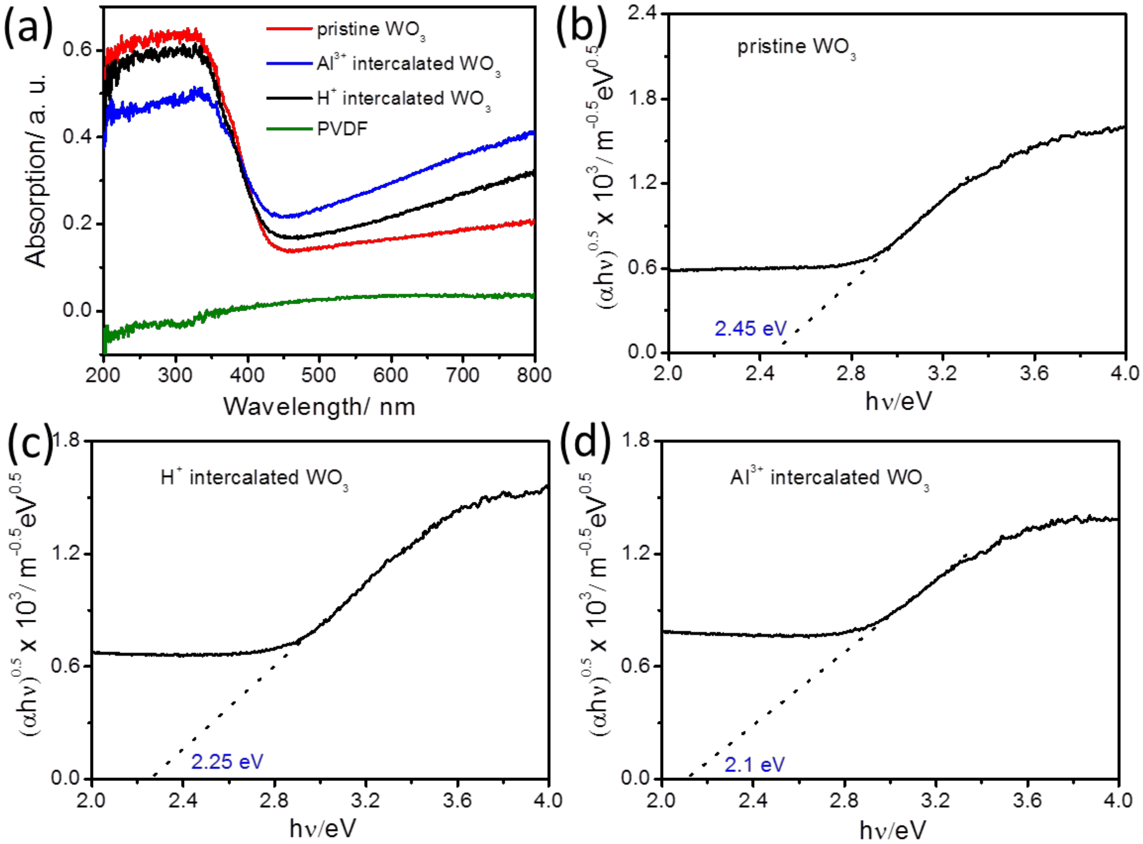

Figure S16: (a) UV-visible absorption spectra of pristine WO_3, Al^{3+} ion intercalated WO_3, H^+ intercalated WO_3 and PVDF. Band gap energy estimation using Tauc equation for (b) pristine WO_3, (c) H^+ intercalated WO_3 and (d) Al^{3+} ion intercalated WO_3.